Available online at www.sciencedirect.com
ScienceDirect
Bioorganic & Medicinal Chemistry 16 (2008) 2779–2790
Bioorganic & Medicinal Chemistry

Binding to human serum albumin of zidovudine (AZT) and novel AZT derivatives. Experimental and theoretical analyses☆

Mario A. Quevedo, Sergio R. Ribone, Guillermo N. Moroni and Margarita C. Briñón*

Dpto. Farmacia, Fac. Ciencias Químicas—U.N.C., Córdoba, Argentina

Received 22 November 2007; revised 3 January 2008; accepted 7 January 2008
Available online 11 January 2008

Abstract—This work presents the binding of AZT and nine novel AZT derivatives to human serum albumin (HSA), both defatted (HSA_D) and complexed with fatty acids (HSA_{FA}). The bound fractions and binding site were determined by applying an ultrafiltration procedure, with an increased affinity for the majority of these derivatives to HSA_D being found with respect to that of AZT, while only one derivative exhibited an increased affinity for HSA_{FA}. By means of computational methods, we observed that specific electrostatic interactions are responsible for the increased affinity for HSA_D, while the presence of fatty acids complexed to HSA caused an intense electrostatic repulsion with negatively charged ligands located in Sudlow site I, thus diminishing their bound fractions. A strong relationship between the calculated energetic components and the observed experimental affinity was identified.

1. Introduction

The binding of drugs to plasma proteins is a very important phenomenon, which affects their pharmacokinetic and pharmacodynamic properties.[1] Human serum albumin (HSA, Fig. 1) is the main protein in plasma, and is of utmost importance in the binding of neutral and acidic compounds.[2] HSA is a single polypeptide chain (MW 65–69 kDa) comprised of three domains (I, II, and III), each of which is divided into two subdomains (A and B). The first crystallographic structures of HSA were obtained in 1989 and 1992, thereby providing the basis for the study of the location of ligand binding sites.[3,4] To date, four main binding sites have been described, of which sites I and II bind the largest number of drugs currently used in medicinal therapy.[5]

HSA is capable of binding both endogenous and exogenous compounds, so an interaction between simultaneously bound molecules is to be expected. Fatty acids (FA) supplied by the diet are the most important endogenous ligands bound to HSA under physiological conditions.[6] In the case of the HSA present in plasma, it is commonly found complexed with FA (HSA_{FA}). HSA also occurs in interstitial fluid (IF), where it exerts vital physiological functions such as pressure homeostasis and is also being capable of binding diverse ligands.[7] In contrast, the lipid content in IF is significantly lower than in plasma,[8] so it can be assumed that the HSA in these fluids is present in its defatted state (HSA_D).

The mechanisms that underlie the binding of small molecules to HSA are complex, being dependent on the specific events occurring at the molecular level. However, these have been intensively studied as a consequence of their importance in the design of novel drugs.[9]

The therapeutic efficacy and safety of zidovudine (AZT, **1**, Fig. 2), the first drug approved for the treatment of acquired immunodeficiency syndrome (AIDS), are closely related to its low HSA_D and HSA_{FA} bound fractions (≅12% to HSA_D and 32% to HSA_{FA}).[10] This, together with the rapid hepatic glucuronidation that inactivates AZT,[11] are the main factors determining its short plasma half-life time (≅1 h),[12] resulting in the need to administer high and frequent doses of drug, thereby producing unwanted side effects.[13] Therefore, obtaining novel AZT derivatives with an increased affinity for HSA is a key strategy for improving this drug's suboptimal pharmacokinetic properties.

Based on the concepts presented above, it is clear that when the HSA binding capacity is being analyzed, it is necessary to consider whether the protein is complexed with FA or not, since this feature may be significantly

Keywords: Human serum albumin; AZT derivatives; Ligand binding; Molecular docking; Molecular dynamics; Fatty acids.
☆ Ref. [1].
* Corresponding author. E-mail: macribri@fcq.unc.edu.ar

0968-0896/$ - see front matter © 2008 Elsevier Ltd. All rights reserved.
doi:10.1016/j.bmc.2008.01.007

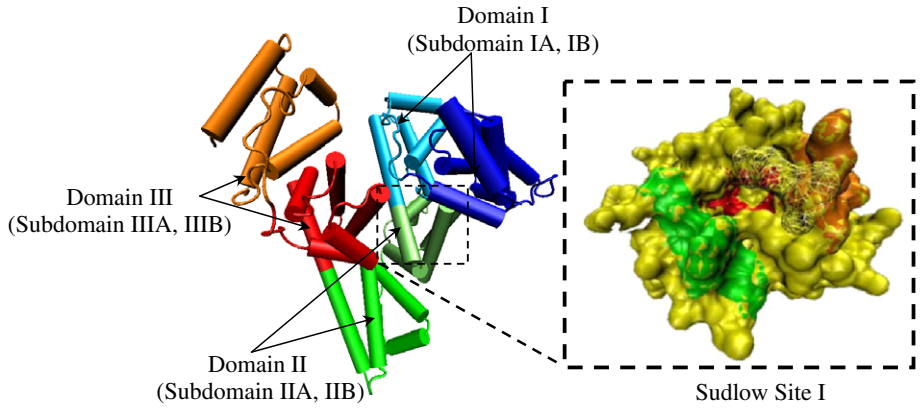

Figure 1. Three-dimensional structure of HSA, with its corresponding domains and subdomains. The enlarged area corresponds to the Sudlow site I binding region.

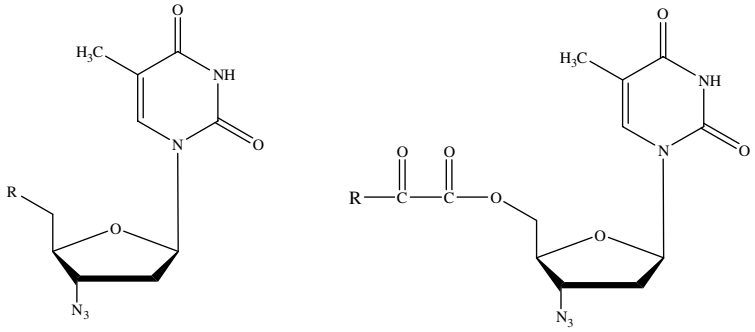

1-AZT; R = OH

2-AZT-Iso; R = OCPy

Compound	R
3-AZT-Leu	$NHCH(COOH)CH_2CH(CH_3)_2$
4-AZT-iLeu	$NHCH(COOH)CH(CH_3)CH_2CH_3$
5-AZT-Pha	$NHCH(COOH)CH_2C_6H_5$
6-AZT-Val	$NHCH(COOH)CH(CH_3)_2$
7-AZT-Trp	$NHCH(COOH)CH_2C_8H_6N$
8-AZT-Pro	NC_4H_7COOH
9-AZT-Tyr	$NHCH(COOH)CH_2C_6H_4OH$
10-AZT-Ac	OH

Figure 2. Chemical structure of AZT and nine novel derivatives whose bound fractions to HSA were studied.

modifying the ligand bound fraction and distribution in the body.

With this in mind, our research group obtained novel prodrugs of AZT (**2**–**10**, Fig. 2),[14–16] designed to enhance its HSA binding affinities. In a previous study, we reported an appropriate methodology to study the binding of six novel prodrugs of AZT to HSA_D, enabling us to identify the binding site of AZT and establish a preliminary structural basis to explain the observed affinity.[17] In the present study, the number of novel prodrugs of AZT assayed was increased when studying the binding to HSA_D, while the effect of the presence of FA was determined by studying the bound fraction of **1**–**10** to HSA_{FA}. In addition, by applying computational methods that included conformational analysis, molecular docking and molecular dynamics simulations, a quali/quantitative structural basis was established in order to explain the observed affinity.

2. Results and discussion

2.1. Binding of AZT and 2–10 to HSA_D and HSA_{FA}

A previously validated ultrafiltration method was applied to study the binding of AZT and **2**–**10** to HSA_D and HSA_{FA}.[17] Tables 1 and 2 show bound fractions (B_f) and affinity constant (K_a) of **2**, **7**–**9**, together with those previously reported (AZT, **3**–**6** and **10**), to HSA_D and HSA_{FA}, respectively. Table 2 also presents the relative difference in their affinity for HSA_{FA} and HSA_D (ΔK_a).

Compounds **2**–**6**, **8**–**10** exhibited an increased bound fraction to HSA_D with respect to that of AZT (Table 1). Compound **10** had the highest affinity with a bound fraction of around four times that of AZT, with compound **7** being the only one that did not exhibit an increase in its bound fraction compared to AZT.

Table 1. Bound fraction (B_f), affinity constant (K_a), and relative affinity (R_A) of **1**–**10** to HSA_D

Compound	HSA_D		
	B_f (%)	K_a (l/mol)	R_A
1-AZT	12.1 (±0.6)[a]	1044.9[a]	1.00
2-AZT-Iso	19.8 (±1.8)	1709.8	1.64
3-AZT-Leu	26.5 (±0.2)[a]	2457.0[a]	2.35
4-AZT-iLeu	35.2 (±0.6)[a]	3765.4[a]	3.60
5-AZT-Val	17.4 (±0.8)[a]	1535.0[a]	1.47
6-AZT-Pha	13.6 (±2.1)[a]	1174.4[a]	1.12
7-AZT-Pro	11.9 (±2.7)	944.6	0.90
8-AZT-Trp	20.5 (±2.1)	1803.2	1.73
9-AZT-Tyr	14.9 (±1.6)	1224.4	1.17
10-AZT-Ac	47.0 (±0.4)	6201.3	5.93

[a] Determined in Ref. 17.

Table 2. Bound fraction (B_f) and affinity constant (K_a) for **1**–**10** to HSA_{FA}

Compound	HSA_{FA}		
	B_f (%)	K_a (l/mol)	ΔK_a[a]
1-AZT	21.2 (±3.2)	1790.7	745.8
2-AZT-Iso	38.8 (±1.0)	3277.3	1567.5
3-AZT-Leu	8.9 (±0.9)	683.2	−1773.8
4-AZT-iLeu	7.6 (±1.1)	575.2	−3190.2
5-AZT-Val	11.9 (±1.8)	944.6	−590.4
6-AZT-Pha	5.5 (±1.7)	436.6	−737.8
7-AZT-Pro	16.1 (±2.0)	1341.9	397.3
8-AZT-Trp	23.7 (±1.0)	2172.1	368.9
9-AZT-Tyr	10.4 (±1.4)	890.9	−333.5
10-AZT-Ac	10.4 (±1.8)	811.7	−5389.6

[a] Difference in affinity between HSA_D and HSA_{FA}.

The effect of FA complexed to HSA for these drug binding modes is considerable, with AZT exhibiting a twofold increase in the bound fraction to HSA_{FA} with respect to HSA_D. The presence of FA also increased the bound fraction of **2**, while **10** exhibited a considerable decrease in its affinity for HSA_{FA}. Among the compounds obtained by combination of AZT with essential aminoacids, the effect of FA was diverse, with a decreased affinity observed for **3**–**6** and **9**, and a slightly increased affinity for **7** and **8**.

By means of displacement studies, we previously reported that AZT binds to the Sudlow site I in the HSA molecule,[17] while in the present work we applied this methodology to identify the binding site of the novel prodrugs (Table 3). In this way, we found that all the studied compounds exhibited a displacement of their bound fractions to HSA_D in the presence of salicylic acid, a Sudlow site I marker, indicating that they were also bound to Sudlow site I.

Based on the experimental data, and considering that both HSA_D and HSA_{FA} are present in the body, two AZT derivatives became of particular interest among the series of studied compounds: **10**, which exhibited a significantly increased bound fraction to HSA_D, and **2**, which exhibited an increased affinity for HSA_{FA}.

In order to understand the features that provided compounds **2** and **10** with these desirable protein binding properties, the search for a qualitative and quantitative model to explain their affinity to HSA_D and HSA_{FA} was initiated, by applying different computational chemistry methodologies (Fig. 3).

Table 3. Bound fraction (B_f) and affinity constant (K_a) to HSA_D in the presence of salicylic acid

Compound	HSA_D + salicylic Acid		
	B_f (%)	K_a (l/mol)	ΔK_a[a]
1-AZT	1.5 (± 0.1)	129.5	−915.4
2-AZT-Iso	nd	nd	nd
3-AZT-Leu	5.2 (±0.8)	449.0	−2008.0
4-AZT-iLeu	4.6 (±2.3)	397.2	−3368.2
5-AZT-Val	15.2 (±1.0)	1312.6	−222.4
6-AZT-Pha	8.3 (±0.5)	716.7	−457.7
7-AZT-Pro	9.4 (±0.8)	811.7	−132.9
8-AZT-Trp	17.6 (±1.1)	1519.8	−283.4
9-AZT-Tyr	9.4 (±1.1)	811.7	−412.7
10-AZT-Ac	7.0 (±0.7)	604.5	−5596.8

[a] Difference in affinity between HSA_D and HSA_D + salicylic acid.

2.2. Structural analysis of Sudlow site I in HSA_D and HSA_{FA}

The structures corresponding to HSA_D (from PDB 1BM0) and HSA_{FA} (from PDB 1E7E) were obtained from crystallographic data,[18] and the topographies of Sudlow site I cavity for each species were compared by analyzing the corresponding affinity grids for carbon and oxygen atoms (see Section 4). From the structural analysis of the site I cavity in HSA_D, two main subpockets were identified, one of a hydrophobic nature (CAV-1) and another of a hydrophilic nature (CAV-2) (Fig. 4).

The presence of FA complexed to HSA induced significant changes in the site I topology (Fig. 5), mainly resulting in an increased volume of the polar mouth of the pocket near CAV-2 (which connects the binding site cavity with the surrounding media), thus making the binding site more accessible. Also, two molecules of

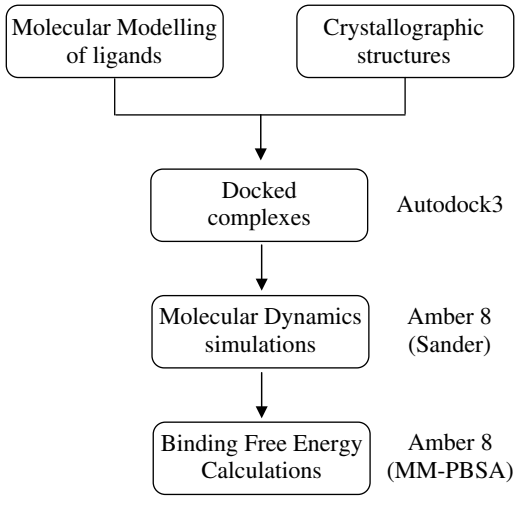

Figure 3. Flowchart of the computational procedures applied to qualitatively and quantitatively study the binding mode of AZT, **2** and **10** to HSA_D and HSA_{FA}.

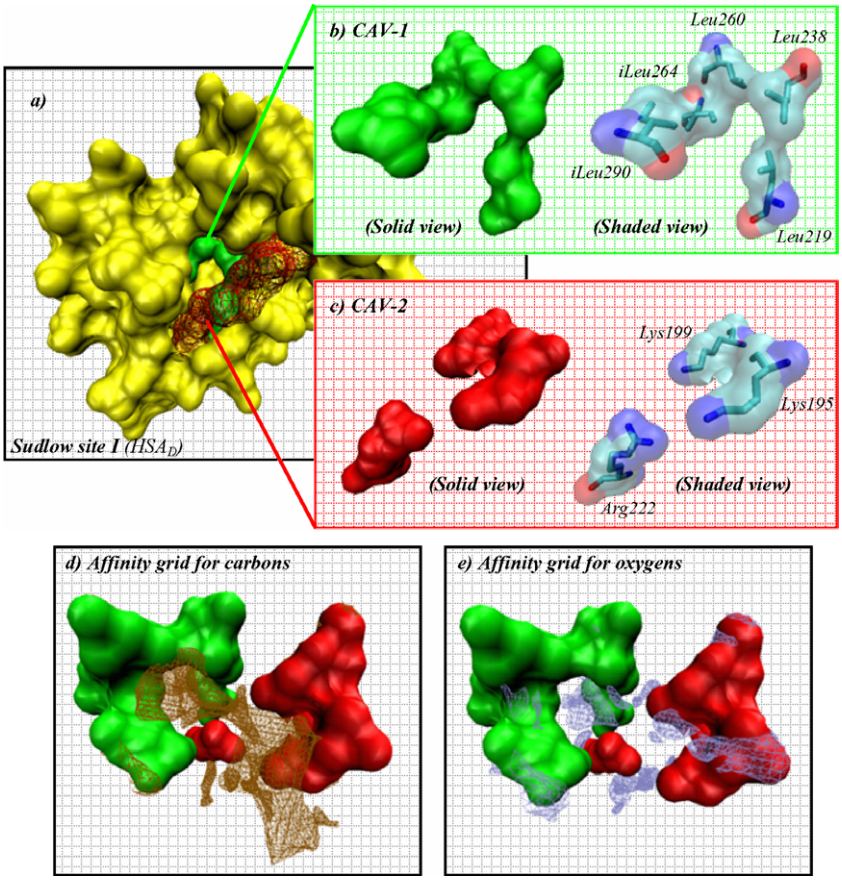

Figure 4. (a) Sudlow site I binding cavity (HSA_D), (b) hydrophobic cavity (CAV-1) inside site I, (c) hydrophilic cavity (CAV-2) located inside site I, (d) and (e) affinity grids for carbons and oxygens, respectively, calculated with Autogrid.

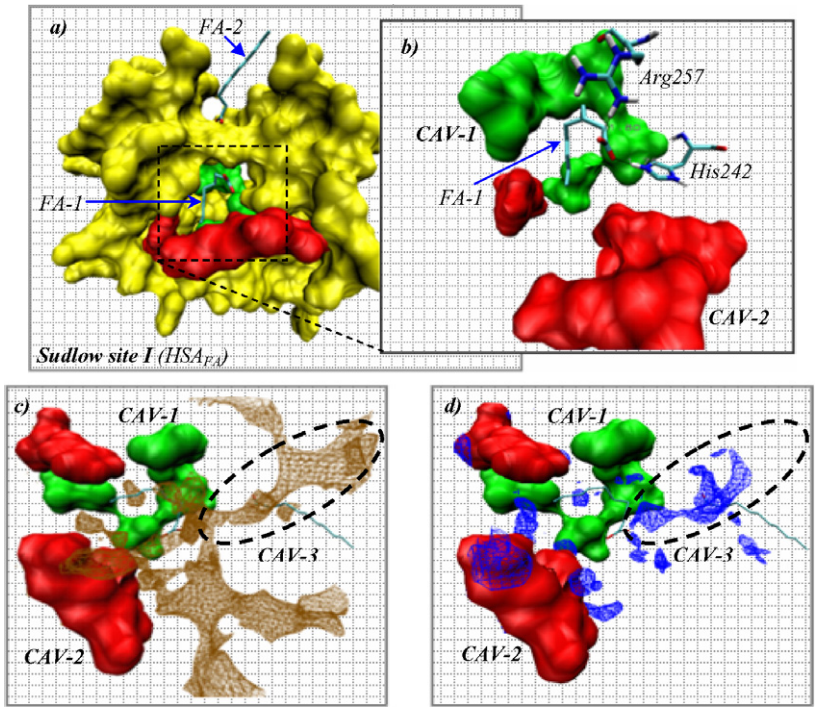

Figure 5. (a) Sudlow site I binding cavity (HSA_{FA}), (b) hydrophobic (CAV-1) and hydrophilic (CAV-2) cavities, showing FA-1 placed inside the binding site, (c) and (d) affinity grids for carbons and oxygens, respectively, indicating the position of CAV-3.

FA were directly associated with the binding cavity in HSA_{FA} (Fig. 5a): FA-1, located inside the binding cavity, with its hydrocarbon chain placed into CAV-1 and its ionized polar head oriented toward the CAV-2 region (Fig. 5b), and FA-2, located outside the binding cavity. This last ligand established ionic interactions with Arg257, thereby producing conformational changes that originated a significant increase in the volume of site I cavity, a fact that has also been previously observed by Ghuman et al.[9] As a consequence of the presence of FA, an additional subcavity within site I was formed, named CAV-3 which is shown in the corresponding affinity grids (Fig. 5c and d).

2.3. Docking studies of AZT, 2 and 10 to HSA_D and HSA_{FA}

In order to obtain the complexes of AZT, **2** and **10** with HSA_D and HSA_{FA}, initial ligand conformations were determined by molecular modeling methods performing systematic conformational searches (Fig. 6). Docking studies were carried out in the region of Sudlow site I, by applying a methodology described in Section 4.

The conformations obtained from the docking procedures were subjected to cluster analysis (see Section 4), after which the clusters corresponding to lowest binding energy (i.e. lowest energy cluster) for AZT, **2** and **10** complexed to HSA_D were obtained (Fig. 7). For simplicity, only the aminoacids surrounding CAV-1 and CAV-2 are displayed, obtained by plotting intermolecular interactions as detected by Ligplot.

From these studies, AZT was found to be located near CAV-2 (Fig. 7a), and established hydrogen bond interactions with Ser192, Gln196, and His242, with sparse hydrophobic contacts. In the complex formed between **2** and HSA_D (Fig. 7b), the AZT template was still

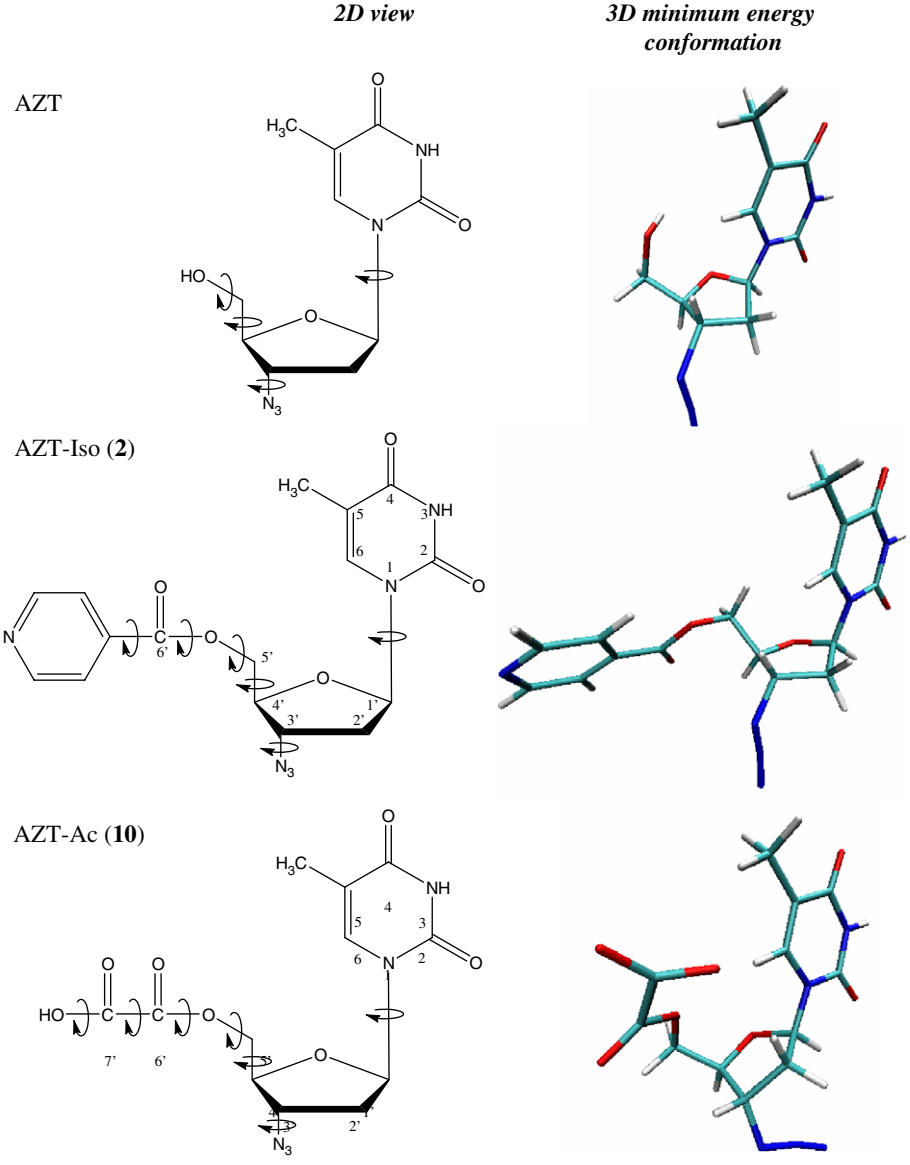

Figure 6. Molecular structure of AZT, **2** and **10**, indicating the rotatable bonds considered in the conformational search (2D view) and the final 3D minimum energy conformation.

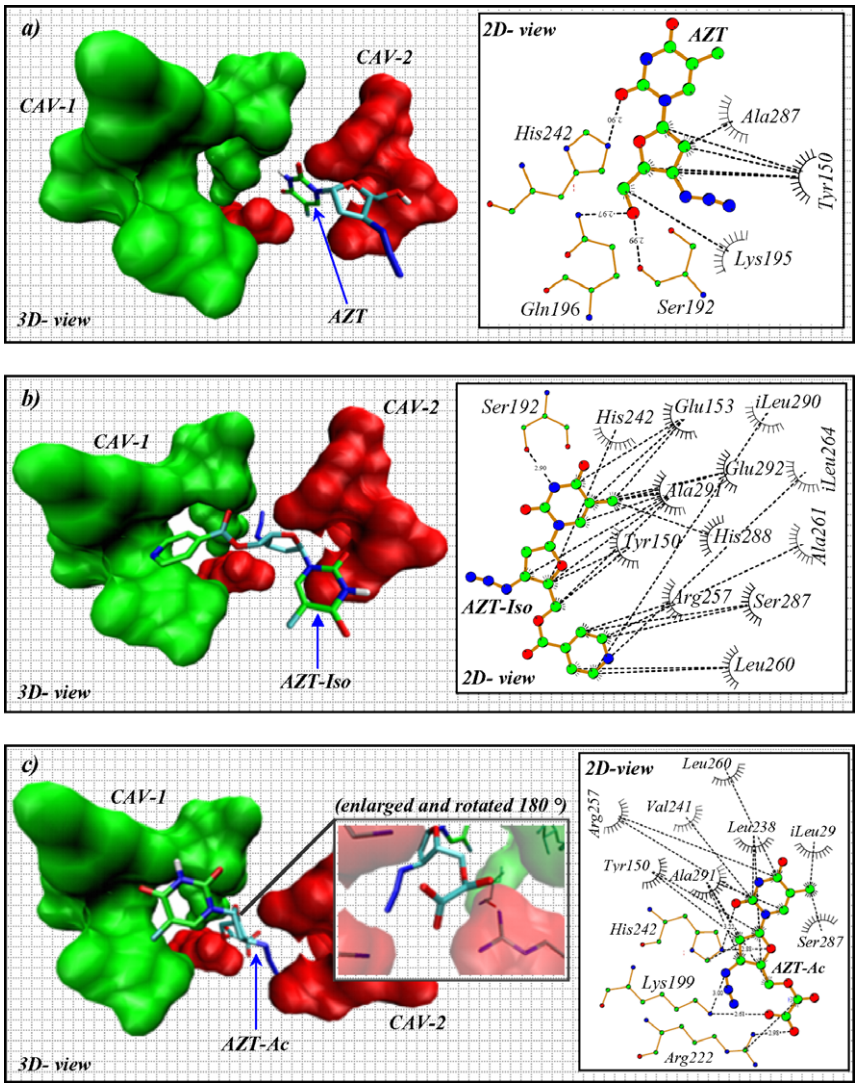

Figure 7. Three-dimensional disposition and plot of the intermolecular interactions of the complexes between: (a) AZT and HSA_D, (b) **2** and HSA_D and, (c) **10** and HSA_D.

located near CAV-2, and had a hydrogen bond interaction with Ser192 along with numerous other Van der Waals interactions. The isonicotinic template of **2**, which conferred to this derivative an increase in lipophilicity and volume with respect to AZT, was oriented toward the hydrophobic cavity CAV-1, and established a high number of Van der Waals interactions as shown by Ligplot.

When analyzing the binding of **10** to HSA_D (Fig. 7c), a critical feature in the formation of the corresponding complex was the stabilization of the negative charge on its carboxyl moiety. This functional group was placed in CAV-2, where it was able to form strong ionic interactions with Lys199 and Arg222, while the AZT template needed to be located in CAV-1 due to conformational restrictions. It also established additional Van der Waals contacts.

From the complexes obtained for AZT, **2** and **10** with HSA_{FA} (Fig. 8), a common feature observed was that CAV-1 was occupied by FA-1, thus the ligands were unable to bind in this region as was the case for HSA_D. When analyzing the binding of AZT (Fig. 8a), it can be seen that the hydrophilic portion of the molecule was still oriented toward CAV-2 and established a hydrogen bond with Gln196. However, since the FA-1 residue was occupying CAV-1, the pyrimidinic moiety was now placed in CAV-3. Compound **2** had the same behavior (Fig. 8b), since CAV-1 was occupied by FA-1. Therefore, the isonicotinic group was now oriented toward CAV-3, forming mainly Van der Waals interactions. When analyzing the complex between **10** and HSA_{FA} (Fig. 8c), we found that although the ionized carboxyl functional group was positioned in CAV-2, the intermolecular interactions plotted show that it was unable to establish ionic interactions with the positively charged aminoacid residues located in this region. The absence of this strong interaction may explain the significant decrease in the affinity of this compound for HSA_{FA} with respect to that for HSA_D (Tables 1 and 2). Similar to the binding mode found for AZT and **2**, the pyrimidinic moiety of **10** was also oriented toward CAV-3 due to the presence of the alkyl chain of FA-1 occupying CAV-1.

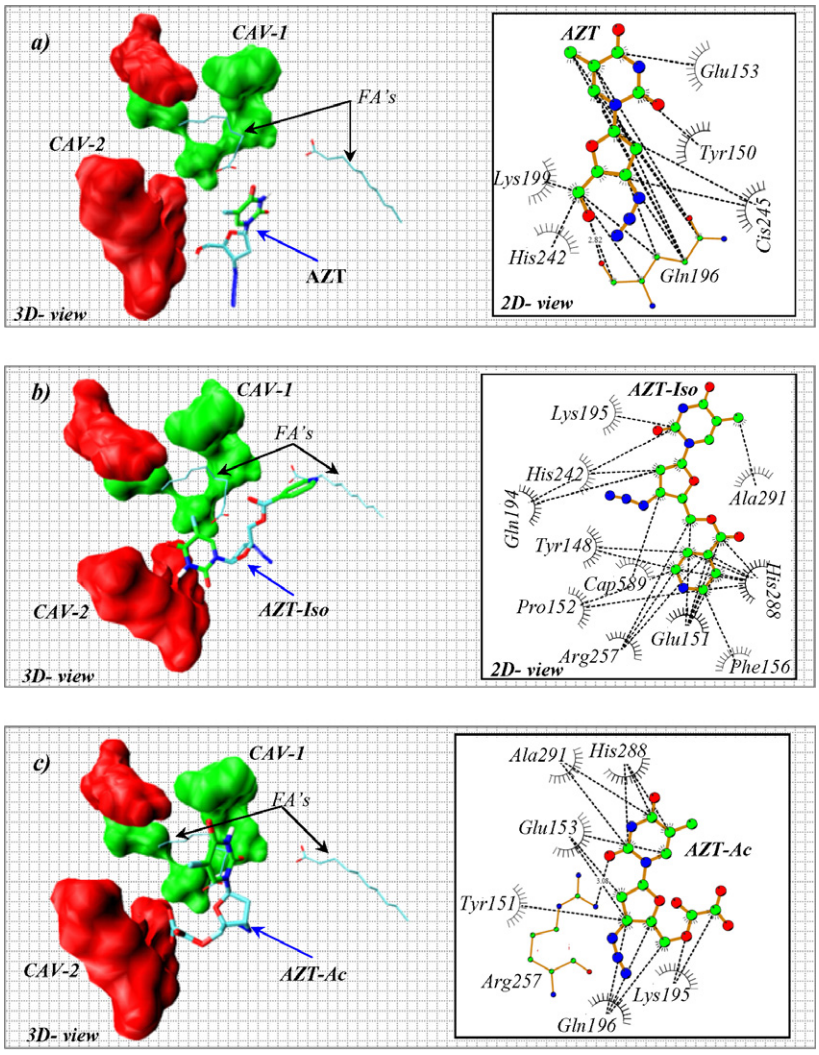

Figure 8. Three-dimensional disposition and plot of the intermolecular interactions of the complexes between: (a) AZT and HSA_{FA}, (b) **2** and HSA_{FA} and, (c) **10** and HSA_{FA}.

Although molecular docking studies were very useful to determine the binding mode of these molecules to both species of HSA, they were unable to provide a robust method to calculate quantitative magnitudes that could be correlated with experimental affinities. This is mainly due to the fact that molecular docking assays did not consider the presence of explicit solvent, or the effect of temperature or protein flexibility in the binding behavior. Thus, to obtain detailed structural and quantitative information that is able to take into account the above-mentioned aspects, the complexes obtained by molecular docking were subjected to molecular dynamics studies.

2.4. Molecular dynamics studies of AZT, 2 and 10 complexed to HSA_D and HSA_{FA}

The protocol described in Section 4 was performed to obtain the corresponding molecular dynamics trajectories. Then, the most occupied interactions were identified and plotted, and based on their corresponding trajectories, their energetic components were calculated through the molecular mechanics Poisson–Boltzmann surface area (MM-PBSA) approach and compared with the experimental affinities of AZT, **2** and **10** for HSA_D and HSA_{FA}.

By analyzing the complex between AZT and HSA_D (Fig. 9), we found that the 5′-OH of AZT acted as hydrogen bond donor and acceptor with Ser192 and Gln196, respectively, with both of them having a considerable occupancy percentage (61.5% and 40.4%, respectively). The carbonyl functional group of the pyrimidinic template in AZT also established a hydrogen bond interaction with His242, while the overall hydrophobic contacts were varied. For the energetic component analysis, we found electrostatic and Van der Waals components of −14.33 and −31.71 kcal/mol, respectively. In this way, we determined that the force driving the binding of AZT to HSA_D originated mainly in hydrophobic contacts, with a relatively low electrostatic component, thus explaining the low bound fraction quantified (12.1%). On analysis of the results obtained for the AZT-HSA_{FA} complex (Fig. 10), and after calculating the associated energetic components, we found a Van der Waals component of −31.85 kcal/mol. This was

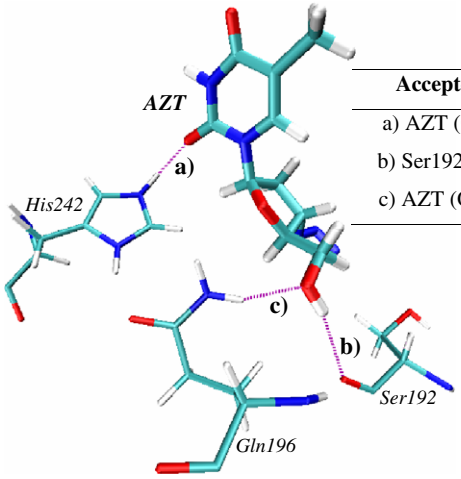

Acceptor	Donor	Occup. (%)
a) AZT (O2)	His242 (N-H)	67.1
b) Ser192 (O)	AZT (O5'-H)	61.5
c) AZT (O5')	Gln196 (N-H)	40.4

Electrostatic comp.	-14.33 (Kcal/mol)
V. der Waals comp.	-31.71 (Kcal/mol)
Total	-46.04 (Kcal/mol)

Figure 9. Intermolecular interactions between AZT and HSA_D and their corresponding energetic components calculated from the molecular dynamics trajectories.

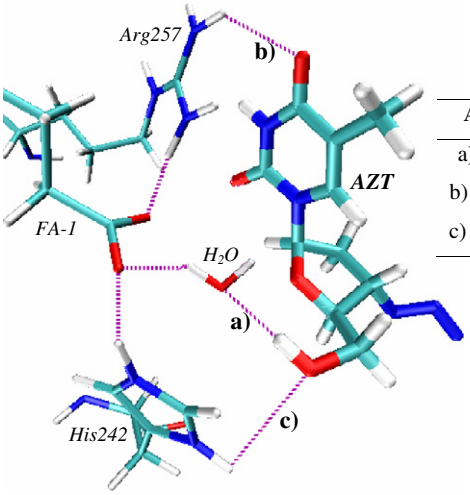

Acceptor	Donor	Occup. (%)
a) H_2O (O)	AZT(O5´-H)	53.3
b) AZT (O4)	Arg257 (N-H)	33.5
c) AZT(O5')	His242 (N-H)	20.9

Electrostatic comp.	1.62 (Kcal/mol)
V. der Waals comp.	-31.85 (Kcal/mol)
Total	-30.23 (Kcal/mol)

Figure 10. Intermolecular interactions between AZT and HSA_{FA} and their corresponding energetic components calculated from the molecular dynamics trajectories.

not significantly different from the value calculated for AZT-HSA_D. Hydrogen bond analyses showed that the 5′-OH group interacted with His242 through a regular hydrogen bond interaction and also with the polar head of FA-1 via a water-mediated hydrogen bond. Considering the high mobility of water molecules, it can be assumed that the geometry of this last interaction is efficiently optimized, thus conferring a high stabilization to the complex. After computing the electrostatic component, we found that the higher affinity observed experimentally for AZT-HSA_{FA} with respect to AZT-HSA_D (Tables 1 and 2) was not reflected in a more negative electrostatic component. This underestimation is ascribed to the fact that the MM-PBSA methodology does not consider the presence of explicit solvent molecules; thus the stabilization produced by the observed water-mediated hydrogen bond is not taken into account.

The trajectories of **2** complexed with HSA_D (Fig. 11) showed that only one hydrogen bond interaction with His242 was found to have considerable occupancy, with its overall electrostatic component being −13.6 kcal/mol. When analyzing the Van der Waals component, we found that it was higher than that of AZT (−52.7 and −31.71, respectively), which provided evidence that the increase in the bound fraction of **2** compared to that of AZT was due to the additional hydrophobic contacts that the isonicotinic template was able to establish in CAV-1. When FA were complexed to HSA, the isonicotinic template was reoriented from CAV-1 to CAV-3 (Fig. 12), with a slight increase occurring in the Van der Waals component (−58.6 kcal/mol). As a consequence of this reorganization, the pyrimidinic portion of this derivative was able to establish an additional hydrogen bond with Arg218, evident by the twofold increase in its electrostatic component compared to that of HSA_D (−28.5 kcal/mol).

From the trajectories for the complexes of **10** with HSA_D and HSA_{FA} (Figs. 13 and 14, respectively), and by analyzing the energetic components corresponding to the former, we found a significantly increased electrostatic component (−163.4 kcal/mol), which derives from

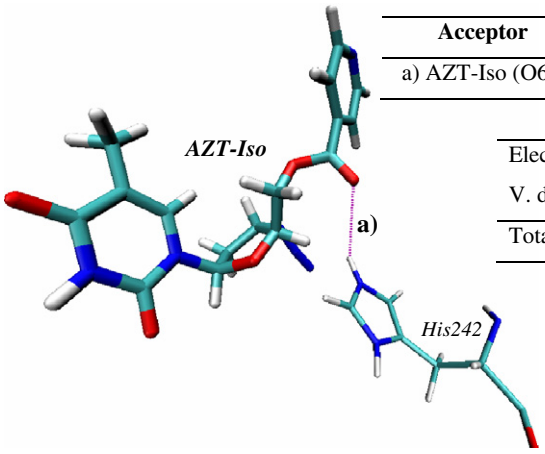

Acceptor	Donor	Occup. (%)
a) AZT-Iso (O6')	His242 (N-H)	74.9

Electrostatic comp.	-13.6 (Kcal/mol)
V. der Waals comp.	-52.7 (Kcal/mol)
Total	-66.3(Kcal/mol)

Figure 11. Intermolecular interactions between **2** and HSA_D and their corresponding energetic components calculated from the molecular dynamics trajectories.

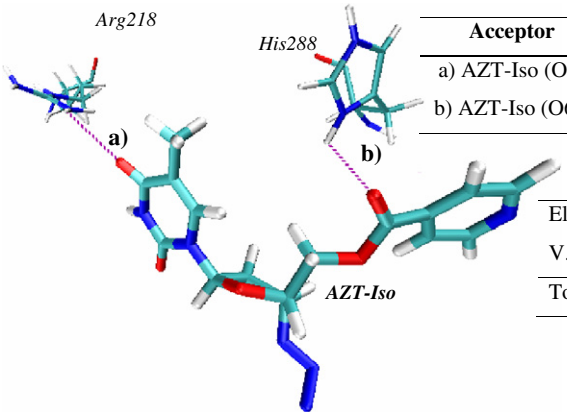

Acceptor	Donor	Occup. (%)
a) AZT-Iso (O4)	Arg218 (N-H)	49.3
b) AZT-Iso (O6')	His288 (N-H)	48.7

Electrostatic comp.	-28.5 (Kcal/mol)
V. der Waals comp.	-58.6 (Kcal/mol)
Total	-87.1 (Kcal/mol)

Figure 12. Intermolecular interactions between **2** and HSA_{FA} and their corresponding energetic components calculated from the molecular dynamics trajectories.

Acceptor	Donor	Occup. (%)
a) AZT-Ac (O4)	Arg257 (N-H)	88.7
b) AZT-Ac (O^-7')	Arg218 (N-H)	56.7

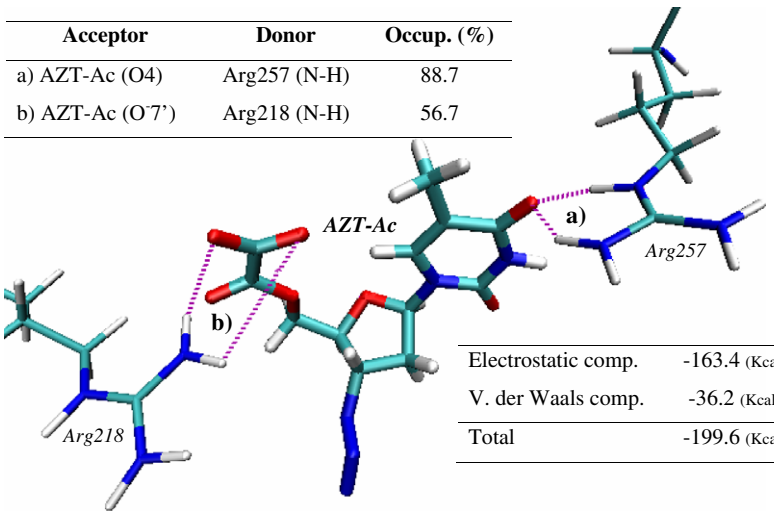

Electrostatic comp.	-163.4 (Kcal/mol)
V. der Waals comp.	-36.2 (Kcal/mol)
Total	-199.6 (Kcal/mol)

Figure 13. Intermolecular interactions between **10** and HSA_D and their corresponding energetic components calculated from the molecular dynamics trajectories.

a strong ionic interaction between the ionized carboxyl moiety of **10** and Arg218, and also a highly occupied hydrogen bond interaction with Arg257. Considering that the Van der Waals component of **10** is not significantly different from that of AZT, we can assume that the considerably increased bound fraction of **10** to HSA_D (47%) was due to the above-mentioned electrostatic interactions. On analysis of the complex of **10** with HSA_{FA} (Fig. 14), we found that the Van der Waals component showed no significant variation with respect to

Acceptor	Donor	Occup. (%)
a) AZT-Ac (O2)	Arg257 (N-H)	57.8
b) AZT-Ac (O7')	Lys199 (N-H)	14.9

Electrostatic comp.	10.2 (Kcal/mol)
V. der Waals comp.	-32.6 (Kcal/mol)
Total	-22.4 (Kcal/mol)

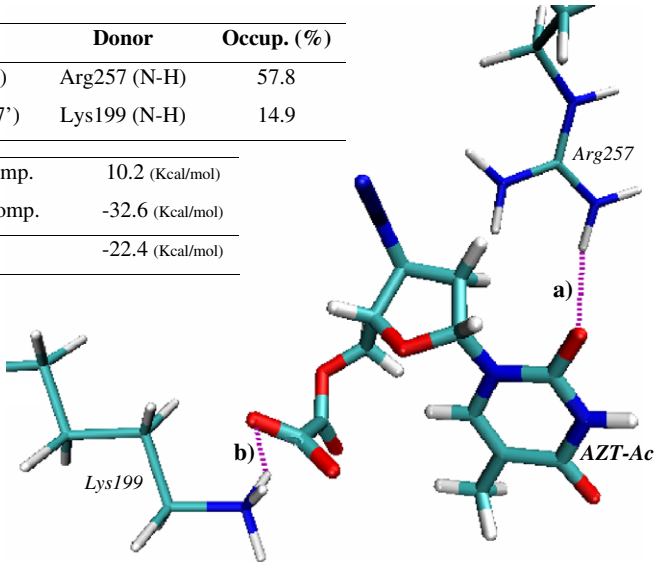

Figure 14. Intermolecular interactions between **10** and HSA_{FA} and their corresponding energetic components calculated from the molecular dynamics trajectories.

HSA_D. However, the stabilization of the complex due to the electrostatic component was considerably diminished, exhibiting a positive value (10.2 kcal/mol), which derived from the electrostatic repulsion between the negatively charged carboxyl moiety of **10** and the FA-1 polar head located in CAV-2. This electrostatic repulsion explains the considerable decrease in the bound fraction of **10** to HSA_{FA} (10.4%).

2.5. Relationship between energetic components and binding affinity

We found a strong relationship between the sum of the calculated electrostatic and Van der Waals energetic components with the corresponding experimental affinity constant, K_a (Fig. 15). The only outlier observed corresponded to the AZT-HSA_{FA} complex, and as mentioned before, this derived from the presence of a water-mediated hydrogen bond interaction that was not taken into account by the MM-PBSA calculation method.

3. Conclusions

The binding of drugs to HSA is a key biochemical phenomenon that determines their eventual fate in the organism. The studies presented in this work have established the structural bases for the binding of AZT to HSA_D and HSA_{FA}. By studying the binding properties of a series of novel AZT derivatives with different HSA bound fractions, we were able to conclude that their affinity for HSA_D was mainly favored by ionic

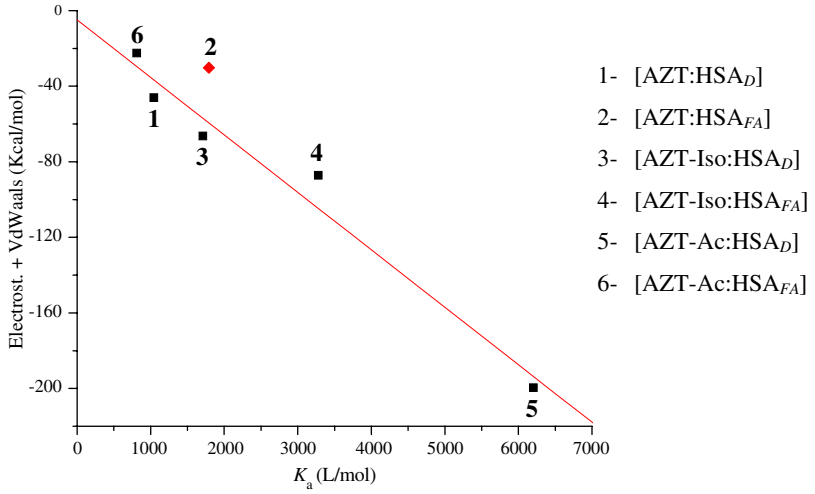

Electrost.+VdW = -0.030 (± 0.003) K_a - 4.93 (± 10.16)

r = 0.9848; R^2 = 0.9643; sd = 13.78; n = 5; F = 578.3

Figure 15. Relationship between the affinities constants (K_a) for AZT, **2** and **10** to HSA_D and HSA_{FA} and the sum of the calculated energetic components.

interactions with the positively charged aminoacidic sidechains present at Sudlow site I. This fact may explain the general observation that HSA preferably binds drugs of a neutral and acidic nature.[1]

The modification of the HSA binding capacity exerted by FA has been long known, and their binding effects on site I have been previously speculated upon.[9] In the present work, we quantitatively demonstrate that FA produces an intense electrostatic repulsion with negatively charged ligands, while the binding of neutral compounds such as AZT and **2** is favored through an electrostatic effect derived from the conformational changes induced in the binding site. This observation also explains the cooperativity observed by FA and warfarin in the bound fraction to Sudlow site I.[19]

From the point of view of the design of novel derivatives of AZT with an increased bound fraction to HSA, the results obtained constitute a basis for the synthesis of new molecules with enhanced affinity for both HSA_D and HSA_{FA}. In this way, it is clear that the presence of a negatively charged group in the new derivative increases its affinity through ionic interactions with positively charged aminoacid sidechains. However, under physiological conditions where HSA is complexed with FA, this property introduces a significant electrostatic repulsion between the FA polar head and the negatively charged molecules located inside the binding site.

Finally, the effects on the pharmacokinetic properties of **2**–**10**, derived from the differential affinity due to both species of HSA (HSA_D and HSA_{FA}), still need to be evaluated through in vivo studies.

4. Experimental

4.1. Apparatus

High performance liquid chromatography (HPLC) assays were performed with an Agilent S1100 chromatograph with UV detection, using an Alltech Allsphere C18-Hypersil 10 μm, 250 × 4.6 mm column. A Haake-DS thermostat bath (±0.1 °C) was used for assays requiring temperature control and a Crison GLP-21 pH meter for pH measurements. A Rolco centrifuge was utilized for ultrafiltration procedures and a TestLab Ultrasonic Cleaner for sample preparation.

4.2. Materials

AZT was obtained from Filaxis Laboratories (Buenos Aires, Argentina), while compounds **2**–**10** were prepared as previously reported.[14–16] HSA was obtained from the Laboratorio de Hemoderivados (U.N.C.). HSA_D was purified by applying a methodology previously reported in the literature,[20] and HSA_{FA} was obtained by adding sodium caprylate to HSA_D and incubating it at 37 °C for 1 h. Phosphate buffer solutions (0.05 M) were prepared prior to use and adjusted to pH 7.4. All other chemicals and reagents were of analytical grade.

4.3. Stock solutions

AZT and **2**–**10** stock solutions were prepared in pH 7.4 potassium phosphate buffer (0.05 M) to obtain the final working concentration (3.0×10^{-5} M). HSA_D and HSA_{FA} stock solutions were prepared as described above to reach the final working concentration of 1 g%. Salicylic acid stock solution was prepared in potassium phosphate pH 7.4 buffer (0.05 M) and diluted to obtain the working concentration (6.0×10^{-5} M).

4.4. Chromatographic conditions and calibration graphs

The mobile phase was a potassium phosphate pH 7 buffer (0.05 M)/MeOH/THF (78:20:2) mixture. Chromatographic runs were performed at 1 ml/min and 25 °C, by injecting 20 μl of solution. Assays were performed with an Agilent S1100 chromatograph with UV detection at 267 nm, using an Alltech Allsphere C18-Hypersil 10 μm, 250 × 4.6 mm column. The corresponding calibration curve was constructed, and a linear response was found in the concentration range 5.0×10^{-6}–1.5×10^{-4} M. The limits of detection and quantitation were 5.18×10^{-7} M and 1.04×10^{-6} M, respectively.

4.5. Drug binding assay

The binding assay procedure was previously validated and reported.[17] Briefly, 5 ml of stock solution of HSA was incubated with 5 ml of **1**–**10** stock solutions at 0 °C for 30 min. After incubation, 1 ml was withdrawn and subjected to ultrafiltration, using a Centrifree® device (MPS-1-Amicon). This was centrifuged for 10 min (2000 rpm) to obtain 0.25 ml of ultrafiltrate. Displacement assays were performed using salicylic acid as the site I marker.[5] All assays were performed in quadruplicate.

4.6. Sample preparation

As previously reported, **2**–**10** were quantitatively hydrolyzed after the ultrafiltration procedure but before the HPLC analysis,[17] thus quantifying the AZT generated from the prodrug hydrolysis. To do this, 0.2 ml of pH 10 sodium bicarbonate buffer (0.05 M) was added to 0.1 ml of ultrafiltrate and the solution was sonicated for 40 min. This was then stored at room temperature for 24 h prior to analysis and confirmed by TLC that the prodrug was completely hydrolyzed.

4.7. Computational studies

X-ray structures of HSA_D (1BM0) and HSA_{FA} (1E7E) were obtained from the ProteinDatabank,[18] while initial ligand conformations were obtained after a systematic conformational search (Fig. 6) using semiempirical (AM1) and ab initio (HF-6-31G*) methods implemented in Gaussian 98.[21,22]

To obtain the ligand–macromolecule complex, molecular docking studies were performed using the AutoDock3 software and prepared with the graphical user interface AutodockTools,[23] with grid maps of

$70 \times 70 \times 70$ points (grid spacing 0.375 Å) centered on Arg257 being calculated with Autogrid3.

A Lamarckian genetic algorithm (LGA) was used to generate ligand populations, while restrained electrostatic potential (RESP) fitted charges were used for the ligand. The integrity of HSA structures was checked with the Amber 8 package, and charges implemented in the FF99 force field were then assigned. The resulting conformations were clustered using a root-mean-square deviation (rmsd) of 2.0 Å, and these were ranked in order of lowest binding energy (referred to as *lowest energy cluster*), with the intermolecular interactions being plotted with Ligplot v.4.4.2.[24] The complexes obtained were subjected to molecular dynamics studies using the Amber 8 package in a system containing explicit TIP3P waters,[25] applying the SHAKE algorithm and a time step of 2 fs. The complexes were simulated for 3 ns, after which structural, hydrogen bond, and energetic component analyses were performed using the Ptraj and Molecular Mechanics Poisson–Boltzmann Surface Area (MM-PBSA) modules of Amber 8.[26] Molecular dynamics simulations were carried out at the Fimm Cluster resource (Parallab, Bergen Center for Computational Science, University of Bergen, Norway).

Acknowledgments

The authors gratefully acknowledge the Secretaria de Ciencia y Técnica de la Universidad Nacional de Córdoba (SECYT-UNC) and the Consejo Nacional de Investigaciones Científicas y Tecnológicas (CONICET) of Argentina for financial support. The authors also wish to express their sincere thanks to Dr. L. Alassia (FILAXIS Laboratories) for supplying AZT and the Laboratorio de Hemoderivados (UNC) for providing HSA. We would also like to specially thank Dr. Petter Bjorstad (Research Director at Bergen Center for Computational Science (BCCS)) for kindly providing access to the BCCS computing resources. Mario A. Quevedo also acknowledges the receipt of fellowships granted by SECYT-UNC and CONICET.

References and notes

1. Shargel, L.; Yu, A. In *Applied Biopharmaceutics and Pharmacokinetics*, 4th ed.; McGraw-Hill, 1999; pp 281–324.
2. Welling, P. G.. In *Pharmacokinetics. Processes, Mathematics, and Applications*; American Chemical Society (ACS): Washington, 1997; pp 119–143.
3. Carter, D. C.; He, H. M.; Munson, S. H.; Twigg, P. D.; Gernert, K. M.; Broom, M. B.; Miller, T. Y. *Science* **1989**, *244*, 1195.
4. He, X. M.; Carter, D. C. *Nature* **1992**, *358*, 209.
5. Peters, T., Jr. In *All About Albumin*; Academic Press: New York, 1995; pp 76–132.
6. Bhattacharya, A. A.; Grune, T.; Curry, S. *J. Mol. Biol.* **2000**, *303*, 721.
7. Smith, D. A.; Van de Waterbeemd, H.; Walker, D. K.; Mannhold, R.; Kubinyi, H.; Timmerman, H. In *Pharmacokinetics and Metabolism in Drug Design*; Wiley-VCH, 2001; pp 47–57.
8. Parini, P.; Johansson, L.; Broijersen, A.; Angelin, B.; Rudling, M. *Eur. J. Clin. Invest.* **2006**, *36*, 98.
9. Ghuman, J.; Zunszain, P. A.; Petitpas, I.; Bhattacharya, A. A.; Otagiri, M.; Curry, S. *J. Mol. Biol.* **2005**, *353*, 38.
10. Luzier, A.; Morse, G. D. *Antiviral Res.* **1993**, *21*, 267.
11. Moore, K. H.; Raasch, R. H.; Brouwer, K. L.; Opheim, K.; Cheeseman, S. H.; Eyster, E.; Lemon, S. M.; Van der Horst, C. M. *Antimicrob. Agents Chemother.* **1995**, *39*, 2732.
12. Warnke, D.; Barreto, J.; Temesgen, Z. *J. Clin. Pharmacol.* **2007**, *47*, 1570.
13. De Clercq, E. In *Drug Discovery and Design: Medical Aspects*; Matsoukas, J., Mavromoustakos, T., Eds.; IOS-Press, 2002; pp 272–278.
14. Motura, M. I.; Moroni, G. N.; Teijeiro, S. A.; Salomon, H.; Briñón, M. C. *Nucleosides Nucleotides Nucleic Acids* **2002**, *21*, 217.
15. Moroni, G. N.; Bogdanov, P. M.; Briñón, M. C. *Nucleosides Nucleotides Nucleic Acids* **2002**, *21*, 231.
16. Moroni, G. N.; Quevedo, M. A.; Ravetti, S.; Briñón, M. C. *J. Liq. Chrom. Rel. Tech.* **2002**, *25*, 1345.
17. Quevedo, M. A.; Moroni, G. N.; Briñón, M. C. *Biochem. Biophys. Res. Commun.* **2001**, *288*, 954.
18. Berman, H. M.; Westbrook, J.; Feng, Z.; Gilliland, G.; Bhat, T. N.; Weissig, H.; Shindyalov, I. N.; Bourne, P. E. *Nucleic Acids Res.* **2000**, *30*, 235.
19. Petitpas, I.; Bhattacharya, A. A.; Twine, S.; East, M.; Curry, S. *J. Biol. Chem.* **2001**, *276*, 22804.
20. Chen, R. F. *J. Biol. Chem.* **1967**, *242*, 173.
21. Leach, A. R. In *Molecular Modelling. Principles and Applications*, 2nd ed.; Prentice Hall, 2001; pp 457–508.
22. Frisch, M. J.; Trucks, G. W.; Schlegel, H. B.; Scuseria, G. E.; Robb, M. A.; Cheeseman, J. R.; Zakrzewski, V. G.; Montgomery, J. A., Jr.; Stratmann, R. E.; Burant, J. C.; Dapprich, S.; Millam, J. M.; Daniels, A. D.; Kudin, K. N.; Strain, M. C.; Farkas, O.; Tomasi, J.; Barone, V.; Cossi, M.; Cammi, R.; Mennucci, B.; Pomelli, C.; Adamo, C.; Clifford, S.; Ochterski, J.; Petersson, G. A.; Ayala, P. Y.; Cui, Q.; Morokuma, K.; Malick, D. K.; Rabuck, A. D.; Raghavachari, K.; Foresman, J. B.; Cioslowski, J.; Ortiz, J. V.; Baboul, A. G.; Stefanov, B. B.; Liu, G.; Liashenko, A.; Piskorz, P.; Komaromi, I.; Gomperts, R.; Martin, R. L.; Fox, D. J.; Keith, T.; Al-Laham, M. A.; Peng, C. Y.; Nanayakkara, A.; Gonzalez, C.; Challacombe, M.; Gill, P. M. W.; Johnson, B.; Chen, W.; Wong, M. W.; Andres, J. L.; Gonzalez, C.; Head-Gordon, M.; Replogle, E. S.; Pople, J. A.; *Software: GAUSSIAN 98*, Gaussian, Inc.: Pittsburgh, PA, USA, 1998; http://www.gaussian.com.
23. Morris, G. M.; Goodsell, D. S.; Halliday, R. S.; Huey, R.; Hart, W. E.; Belew, R. K.; Olson, A. J. *J. Comp. Chem.* **1998**, *19*, 1639.
24. Wallace, A. C.; Laskowski, R. A.; Thornton, J. M. *Prot. Eng.* **1995**, *8*, 127.
25. Case, D. A.; Cheatham, T. E.; Darden, T.; Gohlke, H.; Luo, R.; Merz, K. M.; Onufriev, A.; Simmerling, C.; Wang, B.; Woods, R. J. *J. Comp. Chem.* **2005**, *26*, 1668.
26. Kuhn, B.; Gerber, P.; Schulz-Gasch, T.; Stahl, M. *J. Med. Chem.* **2005**, *48*, 4040.